



HAL
open science

Elaboration of capsules from Pickering double emulsion polymerization stabilized solely by cellulose nanocrystals

Hanaé Dupont, Valérie Héroguez, Véronique Schmitt

► To cite this version:

Hanaé Dupont, Valérie Héroguez, Véronique Schmitt. Elaboration of capsules from Pickering double emulsion polymerization stabilized solely by cellulose nanocrystals. *Carbohydrate Polymers*, 2021, 279, pp.118997. 10.1016/j.carbpol.2021.118997. hal-03771246

HAL Id: hal-03771246

<https://hal.science/hal-03771246>

Submitted on 8 Sep 2022

HAL is a multi-disciplinary open access archive for the deposit and dissemination of scientific research documents, whether they are published or not. The documents may come from teaching and research institutions in France or abroad, or from public or private research centers.

L'archive ouverte pluridisciplinaire **HAL**, est destinée au dépôt et à la diffusion de documents scientifiques de niveau recherche, publiés ou non, émanant des établissements d'enseignement et de recherche français ou étrangers, des laboratoires publics ou privés.

1 **Elaboration of capsules from Pickering double emulsion** 2 **polymerization stabilized solely by cellulose nanocrystals**

3 Hanaé Dupont^{1,2}, Valérie Héroguez^{2,*}, Véronique Schmitt^{1,*}

4
5 ¹ Centre de Recherche Paul Pascal, UMR 5031 Univ. Bordeaux, CNRS, 115 avenue du Dr
6 Albert Schweitzer, 33600 Pessac, France.

7 ² Laboratoire de Chimie des Polymères Organiques, Univ. Bordeaux, CNRS, Bordeaux INP,
8 UMR 5629, Bordeaux, 16 Avenue Pey-Berland, F-33607 Pessac, France.

9
10 * corresponding authors

11 veronique.schmitt@crpp.cnrs.fr

12 heroguez@enscbp.fr

13 14 **Abstract**

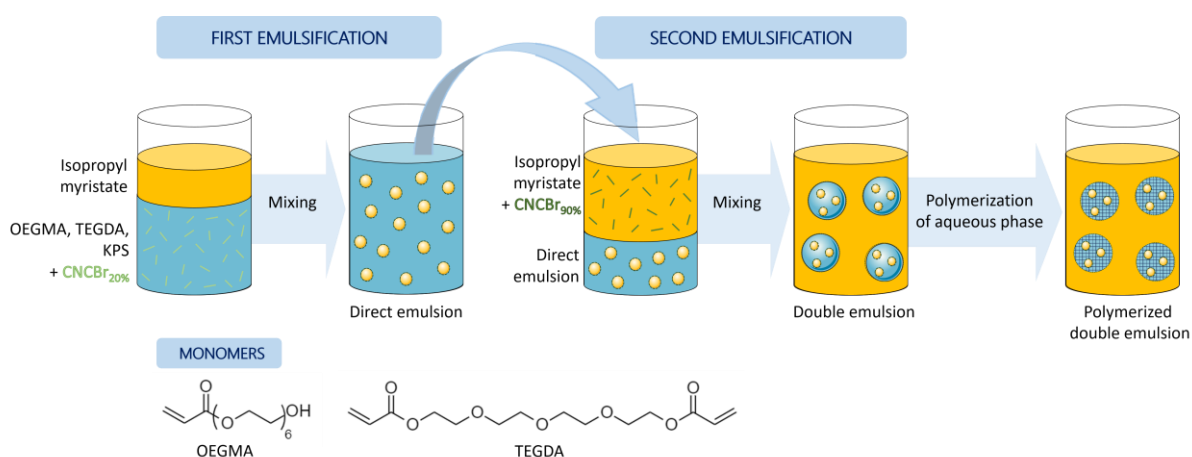
15 Pickering double oil-in-water-in-oil emulsions O/W/O were stabilized using solely cellulose
16 nanocrystals (CNCs), which were modified by introducing surface brominated functions. The
17 emulsions were formulated using only bio-friendly components, among which isopropyl
18 myristate as oil phase, hydroxyl oligoethylene glycol methacrylate (OEGMA) as
19 macromonomer, tetraethylene glycol diacrylate (TEGDA) as cross-linker, and CNCs as
20 stabilizing particles. Formulation parameters could be tuned easily to modulate the fraction of
21 inner emulsion droplets within the double emulsion drops or change the monomer(s)
22 composition within the aqueous phase. The latter was further polymerized to synthesize matrix
23 capsules. The obtained objects showed good resistance to the vacuum and were efficiently
24 used as promising encapsulation vessels. Both hydrophobic and hydrophilic model dyes were
25 encapsulated, with an encapsulation efficiency of about 90%.

26 Keywords: Pickering, cellulose, oil-in-water-in-oil, polymerization, encapsulation

27 **1. Introduction**

28 Emulsions are metastable systems and are defined as the mixture of at least two immiscible
29 liquids. Therefore, their kinetic stabilization requires the use of stabilizing agents, like
30 surfactants, polymers or particles. A rising interest has been put towards the use of particles
31 and the study of the related Pickering emulsions to replace the widely used (macro)molecular
32 scale surfactants (Arditty et al., 2004; Gonzalez Ortiz et al., 2020). Pickering emulsions were
33 discovered by Pickering (Pickering, 1907) and Ramsden (Ramsden, 1904) in the early 1900's
34 and have regained interest since the 2000's because of their high kinetic stability and ease of
35 implementation. According to rising environmental and transparency concerns, the use of
36 organic particles with natural origin as renewable and harmless stabilizers has been
37 considered (Dupont, Maingret, et al., 2021; Sarkar & Dickinson, 2020). Among them, cellulose
38 nanocrystals (CNCs) appear as particles with high potential because they are biosourced and
39 highly available, they are biodegradable and they exhibit a well-known functionalized structure
40 that offers an easily modifiable surface. Studies have shown that they efficiently stabilize direct
41 oil-in-water (O/W) (Deng et al., 2018; Gestranus et al., 2017; Hedjazi & Razavi, 2018;
42 Kalashnikova et al., 2011; Mackie et al., 2019) and inverse water-in-oil (W/O) (Dupont,
43 Laurichesse et al, 2021 ; Guo et al., 2017; Lee et al., 2013; Zhang et al., 2018) Pickering
44 emulsions. However, the occurrences in the literature of more complex systems such as
45 multiple emulsions are still scarce. In most cases, only one of the two interfaces is stabilized
46 by natural organic particles, the other being stabilized by surfactants. This was indeed the case
47 in the study of Matos *et al.* (Matos et al., 2013) who used starch nanoparticles to stabilize the
48 outer interface of water-in-oil-in-water (W/O/W) emulsions, along with a hydrophobic
49 polyglycerol polyricinoleate (PGPR) for the inner interface. More recently, scarce studies
50 reporting double emulsions stabilized solely by particles with natural origin were published.
51 Spyropoulos *et al.* (Spyropoulos et al., 2019) showed good stability of W/O/W emulsions
52 stabilized by rutin particles for the O/W interface, and nanocellulose for the W/O interface, and
53 Cunha *et al.* (Cunha et al., 2014) formulated an O/W/O (oil-in-water-in-oil) emulsions fully
54 stabilized by cellulose derivatives (CNC and/or CNF). Both works focused on the formulation

55 of the double emulsion system as a proof of concept, but did not use it for any particular
 56 application. The only example of application of such systems was demonstrated by Pan *et al.*,
 57 who used lignin particles to produce a W/O/W double emulsions, which intermediate phase
 58 was further polymerized to produce porous absorbent beads (Pan *et al.*, 2015). Hence, we
 59 here propose to investigate further the potential of Pickering double emulsions stabilized solely
 60 with cellulose nanocrystals as polymeric vessels for encapsulation. CNCs of both interfaces
 61 were submitted to the same modification process, their modification rate being the only variable
 62 to modulate their wettability. In the present work, O/W Pickering emulsion was stabilized using
 63 hydrophilic CNCs. This direct emulsion was then used as dispersed phase for a second
 64 emulsification step to produce an O/W/O Pickering double emulsion stabilized by hydrophobic
 65 CNCs, using isopropyl myristate as a biocompatible oil phase. Based on a preliminary study
 66 conducted on W/O emulsions (Dupont, Laurichesse, *et al.*, 2021), the intermediate aqueous
 67 phase of the double emulsion, composed of hydroxyl oligoethylene glycol methacrylate
 68 (OEGMA) and a potential cross-linker (tetraethylene glycol diacrylate, TEGDA), was
 69 subsequently polymerized by free radical polymerization to obtain solid capsules as
 70 schematically depicted in Figure 1. The resulting objects were further proven efficient
 71 encapsulation vessels for both hydrophobic and hydrophilic model dyes, showing the high
 72 applicative potential of these objects.



73
 74 **Figure 1: Principle scheme for the two-step emulsification and synthesis of the polymerized double**
 75 **O/W/O emulsions.**

76

77 2. Experimental

78 2.1 Materials

79 Pristine CNCs were purchased from The University of Maine, under freeze-dried CNC form,
80 isolated from sulfuric acid hydrolysis of wood pulp. The crystals present initially on their surface
81 both sulfate (1.05 wt% as data from the provider) and hydroxyl functions (3.10 ± 0.11 mmol.g⁻¹
82 of CNC). The initial CNCs exhibited a rod-like shape with estimated dimension of $L=138 \pm 47$
83 nm in length and $l=25 \pm 6$ nm in width based on AFM analysis (Dupont et al., 2020; Dupont,
84 Laurichesse, et al., 2021).

85 Triethylamine (TEA) (Fisher scientific, 99%), α -bromoisobutyryl bromide (Bibb) (ABCR, 98%),
86 dimethylaminopyridine (DMAP) (Sigma Aldrich, 99%) were used for the CNC modification
87 without any purification. Isopropyl myristate (IPM) (98%, Alfa Aesar), an oil allowed for
88 cosmetic applications, was used as received as the oil phase for all the emulsion systems.
89 Hydroxyl oligoethylene glycol methacrylate (OEGMA, $M_n = 360$ g/mol) (Sigma Aldrich),
90 tetraethylene glycol diacrylate (TEGDA) (Sigma Aldrich) were used as macromonomer and
91 cross-linker without purification. Potassium persulfate (KPS) (>99%, Sigma Aldrich) was used
92 as received. Fluorescent yellow (FY131SC) (Dow Chemicals) containing Solvent Red 175,
93 methylene blue (Fluka) and toluidine blue (Acros) were used as fluorescent dyes.

94 2.2 CNC-Br synthesis

95 CNC-Br synthesis was first described by Meng *et al.* (Meng et al., 2008) and Morandi *et al.*
96 (Morandi et al., 2009), modified by Werner *et al.* (Werner et al., 2019) and optimized in the
97 present work. 2 g of CNC and 2 g of DMAP were introduced in a double-wall reactor. After a
98 nitrogen purge, 100 mL of dry DMF were added to the powders under gentle agitation with a
99 magnetic stirrer. The solution was cooled down to 0°C. 8.5 g (1.48 mol/L) of Bibb (reactant)
100 and 4.8 g (1.90 mol/L) of TEA, were added to the solution under vigorous agitation. After 3 h
101 for the least modified and 41 h for the most modified, CNC-Br were precipitated in 200 mL of
102 a mixture of THF/ethanol (50/50_{v/v}), isolated by centrifugation (6000 rpm, 10 min, 15°C) and
103 redispersed in water. For a short modification time, that means a low modification rate (3 h,
104 particles noted CNC-Br_{20%}), the aqueous suspension of CNC-Br was dialyzed against pure

105 water during 7 days with a 1 kDa membrane. For a long modification time, that means a high
106 modification rate (41 h, particles noted CNC-Br_{90%}), the purification procedure was different.
107 THF was subsequently added to the CNC-Br aqueous dispersion before centrifugation, in a
108 ratio 1:1. This step was repeated at least 3 times to remove all unreacted species. For both
109 modification times, the final dispersion in water was freeze-dried to obtain a powder.
110 The grafting was confirmed by CP MAS NMR and FT-IR by following the appearance of the
111 stretching bonds corresponding to the surface ester groups at 1760 cm⁻¹ (ν(C=O)) and 1060
112 cm⁻¹ (ν(C-O)) (Fig. S1, SI). Quantitative evaluation of modification rates was determined by
113 elemental analysis thanks to the mass percentage of bromine and the amount of surface
114 hydroxyl groups (Eq. 1).

$$115 \quad \% \text{ substitution} = \frac{\text{mmol of Br by gram of CNCs}}{\text{mmol of surface hydroxyl functions by gram of CNCs}} = \frac{n_{Br}}{n_{OH}} \cdot 100 \quad \text{Eq. 1}$$

116 with $n_{OH} = 3.10$ mmol/g, estimated in a previous study (Brand et al., 2017).

117 **2.3 Emulsion formulation and characterization**

118 **2.3.1 Direct emulsion**

119 The 3 mL aqueous continuous phase was composed of a polymerization system and CNC-
120 Br_{20%} (ranging from 5 to 25 g/L of dispersed phase). The polymerization system was composed
121 of OEGMA (concentration ranging from 10 wt% to 40 wt% with respect to the aqueous phase),
122 possibly a cross-linker TEGDA (15 mol% compared to the total amount of macromonomer,
123 equivalently 5 wt% compared to the aqueous solution) diluted in salted water (NaCl, 40
124 mmol/L) and the free radical initiator KPS (1 g/100 g (macro)monomer(s)). CNC-Br_{20%} were
125 dispersed in the polymerization medium using an ultrasonic bath for 2 min and a Bioblock
126 vibra-cell equipped with an ultrasonic tip during 15 s (cycles of 3 s “on” at 20 % power and 3 s
127 “off”). 1 mL of IPM was added to the aqueous suspension and mixed using the ultrasonic tip
128 during 15 s (cycles of 3 s “on” at 30 % power and 3 s “off”) to obtain an oil-in-water direct
129 emulsion.

130 Emulsion droplet size distribution was obtained by measuring the diameter of a hundred
131 droplets using ImageJ software processing on optical microscopy images. The droplet surface-
132 average diameter, or Sauter diameter $D_{3,2}$ was calculated as follow (Eq. 2):

$$133 \quad D_{3,2} = \frac{\sum_i N_i D_i^3}{\sum_i N_i D_i^2} \quad \text{Eq. 2}$$

134 Where N_i is the number of droplets with diameter D_i . The standard deviation was also
135 calculated as follow (Eq. 3):

$$136 \quad S = \sqrt{\frac{\sum_1^n (D_i - D_{3,2})^2}{n}} \quad \text{Eq. 3}$$

137 **2.3.2 Double emulsion**

138 The continuous phase was prepared by mixing 3 mL of IPM with CNC-Br_{90%} (ranging from 5
139 to 20 g/L with respect to the amount of direct emulsion) with an ultrasonic bath for 2 min. 1 mL
140 of the previously described direct emulsion was incorporated to the oil-CNC mixture using a
141 vortex at 1500 rpm for 30 s. The double emulsion drop size was assessed identically as for the
142 direct emulsion using Eq. 2 and Eq. 3. In the following, droplet denomination will refer to the
143 inner emulsion, whereas the term drop will refer to the external one.

144 **2.4 Double emulsion polymerization and characterization**

145 The double emulsions were placed in an oil bath at 75°C for 24h. The emulsion drop size
146 distribution after polymerization was controlled by optical microscopy using Eq. 2 and Eq. 3. A
147 sample of the polymerized double emulsions was then washed with EtOH and dried to assess
148 the morphology by scanning electron microscopy (SEM). In the following, the polymerized
149 double emulsions will be referred as capsules.

150 **2.5 Dye encapsulation within the double emulsion**

151 The hydrophobic dye FY131SC was diluted in IPM to reach a concentration of 0.002 wt%. The
152 hydrophilic dye, toluidine blue, was diluted in salted water (NaCl, 40 mmol/L) to reach a
153 concentration of 0.02 wt%. This solution was used for the (macro)monomer(s) dilution to
154 formulate the stained aqueous phase of the emulsion. The direct emulsion was formulated with
155 the two previously described oil and aqueous phases. This emulsion was then incorporated

156 into regular IPM to obtain the double emulsion. Both direct and double emulsions were
157 observed using a confocal microscope equipped to assess the effective encapsulation of both
158 dyes.

159 The encapsulation efficiency (EE) was measured from double emulsions containing only
160 FY131SC in the inner IPM droplets. 500 μL of the continuous supernatant IPM was taken from
161 the double emulsion and diluted in 500 μL of regular IPM. The mixture was then filtered and
162 analyzed by UV-visible spectrophotometry. The EE was calculated as (Eq. 4):

163
$$\text{Encapsulation efficiency (\%)} = \left(1 - \frac{\text{amount of dye in the continuous phase}}{\text{total amount of dye in the double emulsion}}\right) * 100 \quad \text{Eq. 4}$$

164 **2.6 Instrumentation**

165 Infrared spectra of unmodified and brominated CNCs were recorded using a Vertex 70 Bruker
166 FT-IR spectrometer. CNC powder was analyzed thanks to an attenuated total reflectance ATR
167 accessory. Each spectrum was recorded between 4000 cm^{-1} and 400 cm^{-1} with a resolution of
168 4 cm^{-1} with 32 scans.

169 Optical micrographs were taken on a bright-field upright microscope (Zeiss Axioscope 40) with
170 an Axioscope 105 color camera. Emulsions were placed onto a glass slide, then a spacer was
171 used to avoid compression of the droplets during observation, finally the sample was covered
172 by a lamella. The recorded images were analyzed with ImageJ.

173 Scanning electron microscopy (SEM) observations were performed with a HITACHI TM-1000
174 apparatus operating at 15 kV. Samples were coated with a layer of Au-Pd before observation
175 using a plasma at 10 mA for 30 s.

176 All confocal microscopy images were acquired on a Leica TCS SP5 (Leica Microsystems CMS
177 GmbH, Mannheim, Germany) inverted confocal microscope (DMI6000).

178 UV-visible spectrophotometry was performed using a Cary 100 UV-vis spectrophotometer
179 between 400 nm and 800 nm, in 500 μL quartz cells.

180 Contact angles were measured on a Teclis apparatus using the drop deposit technique. Pellets
181 of CNCs were produced from 200 mg of dry material using a 13 mm Evacuable Pellet Die and
182 a manual hydraulic press (5 tons during 1 min). The pellets were kept dry in an oven at 50 $^{\circ}\text{C}$

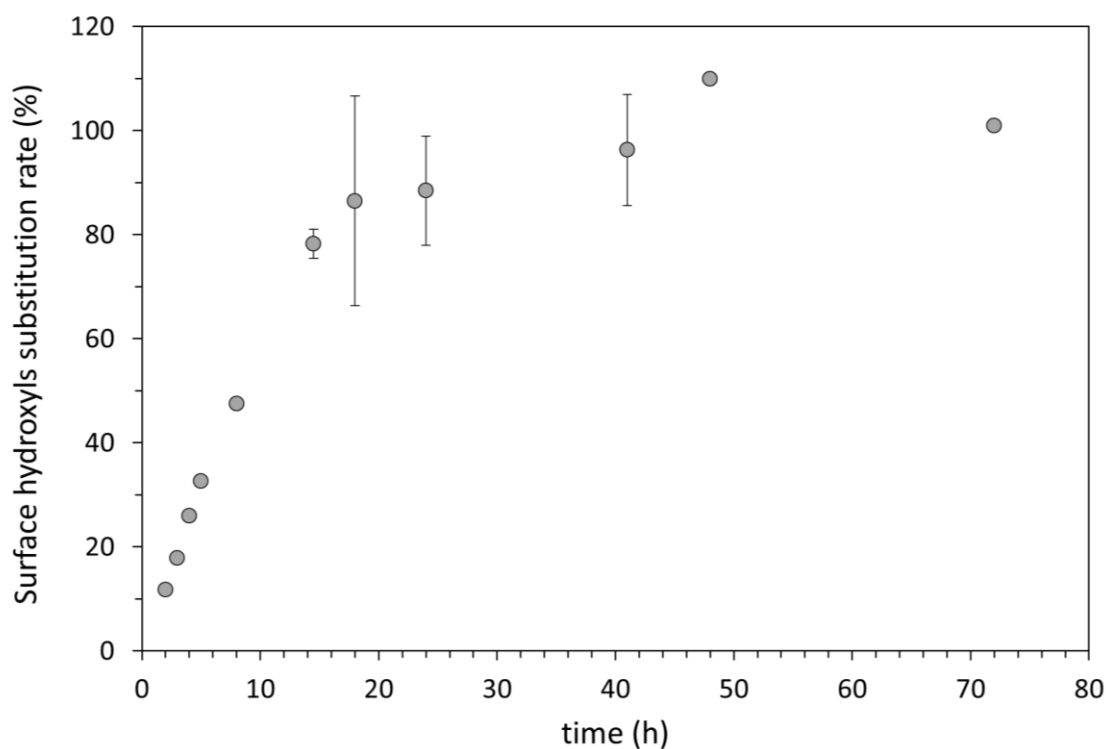
183 prior to experiment. Drops of salted water (4 μ L) were deposited on the pellets and the contact
184 angle was measured. For each CNC modification rate, the contact angle was measured at
185 least three times.

186

187 **3. Result and discussion**

188 **3.1 CNC modification**

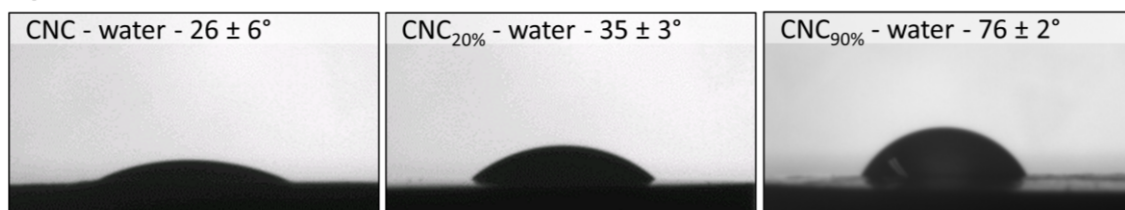
189 The CNC were modified using Bibb, enabling the grafting of brominated moieties often used
190 for the initiation of controlled radical polymerization like ATRP, as demonstrated in a previous
191 study (Dupont, Laurichesse, et al., 2021). Here, the grafting was only used in order to increase
192 the overall hydrophobicity of the CNCs. The CNC modification rate of hydroxyl functions into
193 brominated hydrophobic moieties could be controlled by adjusting the reaction time. The more
194 time the reactants were in contact with the CNCs the more hydroxyl functions were esterified,
195 leading to more hydrophobic CNCs. As a consequence, the modification rate functions could
196 be plotted against the reaction time, showing a linear increase in brominated functions followed
197 by a plateau when reaching 100% of hydroxyl substituted by brominated function for at least
198 40 h of reaction (Figure 2A).



B)

Modification features	CNC-Br _{20%}	CNC-Br _{90%}
Duration of the reaction (h)	3	41
%wt of Br	4.43	21.98
mmol of Br per gram of CNC	0.55	2.75
OH substitution rate at the CNC surface (%)	18	89

C)



199

200 *Figure 2: A) CNC surface modification rate as a function of the reaction time. Error bars represent the*
 201 *repeatability of the experiment for a given reaction time. B) Characteristics of the two modified CNC*
 202 *batches used in this study. C) Contact angle between water, CNC surfaces and air.*

203 It has been observed that for low modification rates (up to 50%), the CNCs were still hydrophilic
 204 enough to be dispersed in water and to stabilize efficiently direct O/W emulsions. Moreover,
 205 the surface modification performed on the CNCs enhanced their ability to adsorb at oil-water
 206 interfaces, making them more suitable Pickering emulsion stabilizers, compared to pristine
 207 crystals. On the contrary, above 50% of modification the CNCs become more hydrophobic and

208 can only be dispersed into hydrophobic solvents or oils (Destribats et al., 2014; Finkle et al.,
209 1923). Following Finkle's law, they indeed efficiently stabilize inverse W/O emulsions.

210 In the present study, we chose to work with two sets of surface-modified CNCs, suitable for
211 the stabilization of direct and inverse emulsions. Two batches of CNCs were therefore modified
212 during 3 h and 41 h respectively to reach modification rates of approximately 20% and 90%
213 (Figure 2A, Figure 2B). They are noted CNC-Br_{20%} and CNC-Br_{90%} respectively.

214 To further characterize the chemical modification and hydrophilic-lipophilic balance of the
215 CNCs, water contact angles were measured for pristine CNCs and the two CNC-Br batches
216 (Figure 2C). Water droplets were deposited onto the CNC pellets, showing an increase in the
217 contact angle with the increase of brominated moieties. Pristine CNCs exhibited a low contact
218 angle of $26 \pm 6^\circ$ consistent with their intrinsic hydrophilic nature. For low modification rate, the
219 contact angle value increased to $35 \pm 3^\circ$, showing that the CNC-Br_{20%} are more hydrophobic
220 than their pristine form, but are still quite hydrophilic, as they can be redispersed in water. On
221 the contrary, for high modification rates as for CNC-Br_{90%}, the contact angle increased by 50°
222 compared to pristine particles, up to $76 \pm 2^\circ$, showing the great impact of the surface
223 modification on the hydrophilic/hydrophobic behavior. It is worth noting that this three-phase-
224 contact-angle was measured between CNCs, water and air, which allows a comparison
225 between the different CNCs but does not give the three phase contact angle of the system
226 used in the emulsions: it is therefore useful as a comparative method but does not represent
227 the present system, as the monomer and the oil are missing from this measurement.

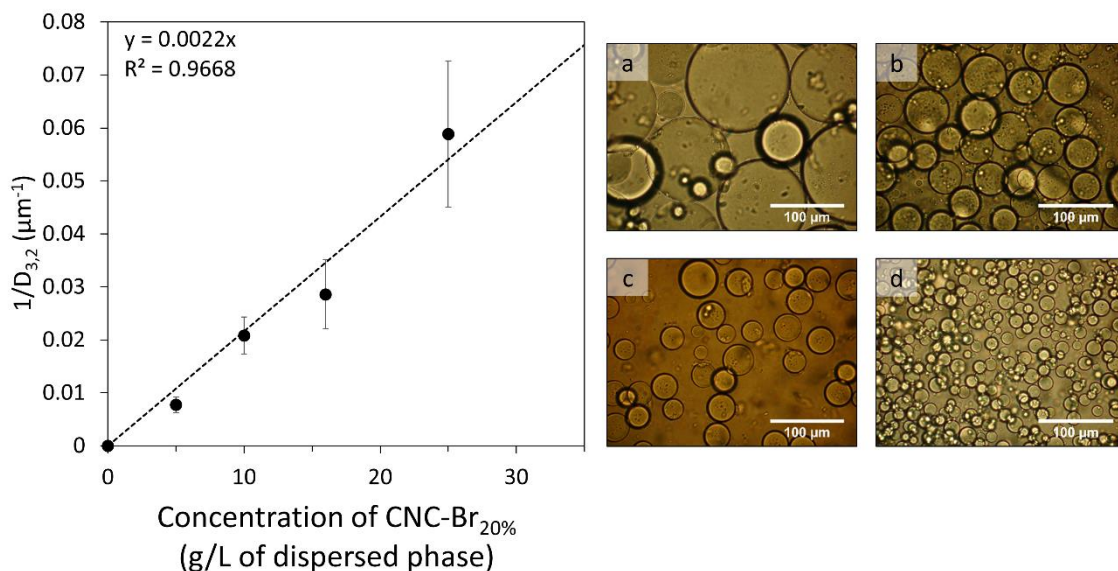
228

229 **3.2 Emulsion formulation**

230 **3.2.1 Direct emulsion O/W**

231 Emulsions components were chosen in order to formulate an overall bio-friendly system. IPM
232 was used as oil phase, as a non-toxic biocompatible oil already used in cosmetic and
233 pharmaceutical applications. Regarding the aqueous phase, the polymerization system was
234 selected similarly using biocompatible functionalized polyethylene glycol derivatives, OEGMA
235 and TEGDA. The metastable emulsion was then stabilized using biosourced CNCs.

236 Emulsion formulation parameters were determined based on previous optimization on simple
 237 inverse emulsions (Dupont, Laurichesse, et al., 2021). Hence, the concentration of OEGMA
 238 was set to 10, 35 or 40 wt% of the aqueous phase, and the possible addition of TEGDA as a
 239 cross-linker was set to 15 mol% with regard to the total (macro)monomers concentration (which
 240 is equivalent to a composition of 35 wt% of OEGMA and 5 wt% of TEGDA with respect to the
 241 aqueous solution). Oil-to-water volume fraction could be tuned, and O/W emulsions were
 242 formulated with fraction of 25/75 or 50/50, which will enable later the variation of inner droplets
 243 concentration for the double emulsion loading.
 244 Stable direct O/W Pickering emulsions were obtained using CNC-Br_{20%} particles as stabilizers,
 245 as they were mainly hydrophilic and could lead to the stabilization of direct emulsion following
 246 Finkle's rule (Finkle et al., 1923). The concentration in OEGMA was set to 40 wt%, and the
 247 concentration in stabilizing particles was varied from 5 to 25 g/L with respect to the oil phase.
 248 The Sauter diameter was measured for each sample and its inverse ($1/D_{3,2}$) was plotted
 249 against the CNC-Br_{20%} concentration (Figure 3).



250
 251 *Figure 3 : Left, Reverse drop diameter as a function of the amount of CNC-Br_{20%} in the aqueous phase.*
 252 *All the other parameters are kept constant: 25/75_{v/v} of IPM/polymerization system, OEGMA 40 wt% no*
 253 *TEGDA. The linear variation highlights the limited coalescence phenomenon occurring in this*
 254 *concentration range. Right, optical microscopy shots of the emulsions with a) 5 g/L, b) 10 g/L, c) 16 g/L,*
 255 *d) 25 g/L of CNC-Br_{20%}.*

256 The plot shows a linear dependence of the inverse of the diameter with the CNC-Br_{20%} particle
 257 concentration, which is characteristic of the behavior of Pickering emulsions. Indeed, in the

258 particle-poor domain, the size can be controlled by the amount of particles thanks to the limited
259 coalescence phenomenon, because of the irreversible adsorption of particles at the oil-water
260 interface (Arditty et al., 2003; Wiley, 1954). From the slope, it is possible to extract the covering
261 ratio (C parameter), which is defined as the proportion of interface covered by particles. The
262 slope is defined as (Schmitt et al., 2014) (Eq. 5):

$$\frac{1}{D_{3,2}} = \frac{m_p}{6\rho_p V_d C} \cdot \frac{a_p}{v_p} \quad \text{Eq. 5}$$

264 where a_p and v_p are the projected surface and the volume of the particles in contact with the
265 interface ($140 \times 25 \text{ nm}^2$ and $140 \times 25 \times 25 \text{ nm}^3$ respectively, approximating the CNC shape to a
266 parallelepiped rectangle), m_p corresponds to the mass of particles, ρ_p their density (taken as
267 1.6 g/cm^3), V_d the volume of the dispersed phase, and C the covering ratio. In the case of
268 CNCs, which can be approximated to parallelepiped particles, a dense monolayer corresponds
269 to a C value of 1. When $C > 1$, the droplets are covered in average by n layers of particles, with
270 $C = n \times 100 \%$. Here from the slope, it can be extracted that emulsions droplets are covered
271 by 2 layers of CNCs in average. The formulation of the direct emulsion allows reaching stable
272 emulsions droplets with mean diameters down to $17 \text{ }\mu\text{m}$, which makes them suitable as inner
273 droplets for the double emulsion formulation. Indeed, previous attempts of formulating simple
274 inverse emulsions of the same composition (water phase composed of 40 wt% of OEGMA)
275 enabled producing droplets of average diameter of $400 \text{ }\mu\text{m}$ (Dupont, Laurichesse, et al., 2021).
276 It can therefore be assumed that the drops size of the second emulsification will be in the same
277 range and thus suitable for the production of nicely defined double emulsions.

278 **3.2.2 Double emulsion O/W/O**

279 Double emulsions containing the monomers were formulated following a two-step
280 emulsification process, with CNC-Br stabilizing each one of the two interfaces. According to
281 previous characterizations, CNC-Br_{20%} were used to stabilize the O/W inner emulsion interface,
282 and CNC-Br_{90%} for the outer interface. The simple direct emulsion was first formulated as
283 described in the section 3.2.1 and used as dispersed phase for the second emulsification. By

284 changing the oil-to-water volume fraction of the direct emulsion, the loading fraction of inner
285 droplets within the double emulsion could be tuned (Eq. 6).

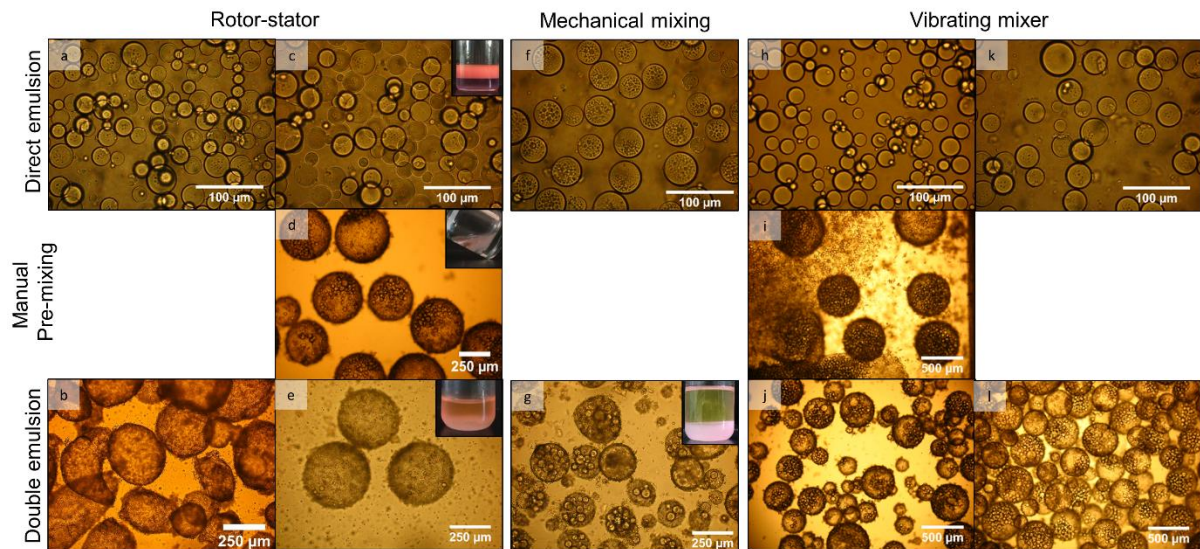
$$286 \quad n_{inner} = \varphi_{oil} \times \frac{D_{4,3}^3}{d_{4,3}^3} \quad Eq. 6$$

287 with n_{inner} the average number of inner droplets, φ_{oil} the oil volume fraction of the direct
288 emulsion, $D_{4,3}$ the volume averaged diameter of the external drops and $d_{4,3}$ the volume-

$$289 \quad \text{averaged diameter of the inner droplets defined as } D_{4,3} = \frac{\sum_i N_i D_i^4}{\sum_i N_i D_i^3}.$$

290 Regarding the process, the choice of the second emulsification was determinant as it must not
291 induce the modification, neither fragmentation nor destabilization of the inner emulsion. As a
292 consequence, several mixing procedures were considered, with shear rates lower than the one
293 induced by the ultrasonic probe used for the first emulsification (Ding et al., 2019). Rotor-stator,
294 mechanical stirring and vibrating mixer were tested. In order to assess the stability of the
295 double emulsion, the oil dispersed in the direct emulsion was stained with Nile Red (solubility
296 in water 0.2 mg/mL), and the repartition of the dye after the second emulsification was used
297 as a macroscopic indicator for process viability. More precisely, if the dye was finally present
298 in the continuous phase, then it was assumed that the innermost and outer oily phases have
299 been in contact during the emulsification process. This has to be avoided to prevent dilution of
300 the active to be encapsulated and as a consequence to prevent low encapsulation efficiencies.
301 At the microscopic scale, double emulsions were observed by optical microscopy and the
302 average number of inner droplets was coarsely compared to the theoretical expected value
303 n_{inner} (Eq. 6). Firstly, a rotor-stator Ultra-turrax[®] emulsification at low power (5000 rpm for 30 s)
304 was employed (Figure 4 a, b). The direct emulsification led to empty double emulsions, similar
305 to inverse emulsions. Therefore, a manual pre-mixing step was added to follow the emulsion
306 evolution step-by-step. After a gentle manual premixing, the external oil was already stained
307 with Nile Red (Figure 4 d), meaning that the emulsification did rupture some of the droplets of
308 the direct emulsion. Regarding the morphology, the effective number of encapsulated inner
309 droplets was already far from the theoretical value of a 250 droplets estimated by Eq. 6. After

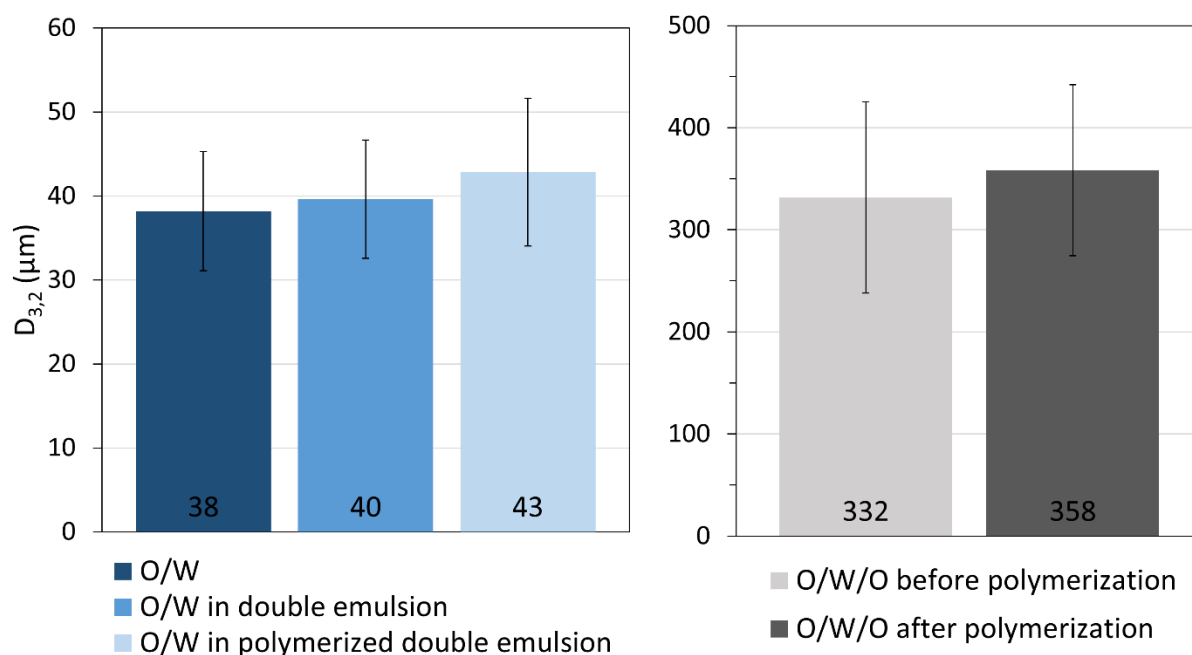
310 further stirring using the Ultra-Turrax® rotor–stator mixer, the staining in the continuous oil
 311 phase intensified, and no inner droplet was visible anymore (Figure 4 e). Similarly, mechanical
 312 stirring ended up in the destabilization of the direct emulsion and an intense coloration was
 313 visible in the continuous phase after the second emulsification step (Figure 4 g).



314

315 *Figure 4 : Process optimization for emulsion formulation. a, b) direct and double emulsions from rotor-*
 316 *stator mixing. c, d, e) direct, premix and double emulsions from rotor-stator mixing. f,g) direct and double*
 317 *emulsions from mechanical stirring. h,i,j) direct, premix and double emulsions from vibrating mixer*
 318 *stirring. k,l) direct and double emulsions from vibrating mixer stirring. The inserts, when present, show*
 319 *the macroscopic aspect of the emulsion containing Nile Red.*

320 Finally, a gentler process was chosen, and emulsification with a vibrating mixer (1500 rpm for
 321 30 s) showed good results upon the double emulsion formulation, provided the suppression of
 322 the manual pre-mixing step (Figure 4 l). The inner emulsion average droplet diameter is
 323 preserved during the emulsification, as it is equal to $38 \pm 7 \mu\text{m}$ before and $40 \pm 7 \mu\text{m}$ after
 324 (Figure 5 left). Moreover, the CNC-Br_{90%} were efficiently adsorbed at the newly created water-
 325 oil interface as no sign of excess particles could be seen in the continuous phase.



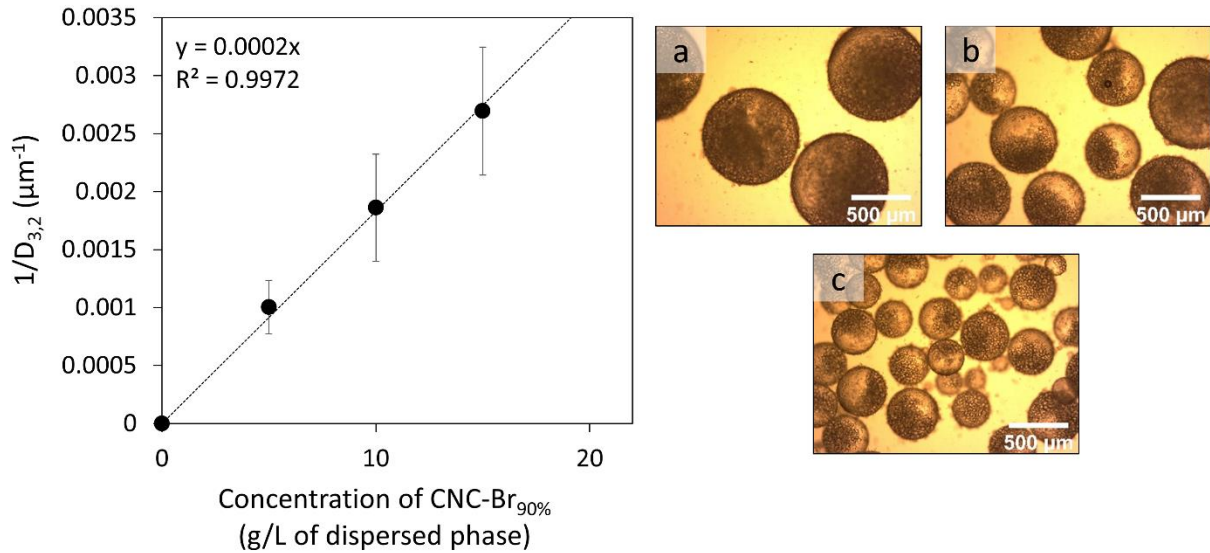
326

327 *Figure 5: Left) inner droplets size distribution evolution after formulation, after incorporation in the double*
 328 *emulsion and after polymerization of the double emulsion. Right) double emulsion size distribution*
 329 *evolution before and after polymerization. The error bars reflect the drops size distribution width*
 330 *(standard deviation).*

331

332 By setting the OEGMA concentration to 40 wt% in the aqueous phase, the concentration of
 333 CNC-Br_{90%} was varied and the according diameter of the double emulsion was measured. By
 334 plotting the inverse of the drop diameter as a function of the concentration of CNC-Br_{90%}, a
 335 linear relationship characteristic of the limited coalescence phenomenon could be evidenced
 336 at the drop scale (Figure 6). In a previous contribution (Dupont, Laurichesse, et al., 2021),
 337 inverse simple emulsions of a 40 wt% OEGMA solution-in-IPM stabilized by CNC-Br_{90%} were
 338 obtained by homogenization with a rotor-stator, Ultra-turrax[®] S18N-10G at 15 000 rpm for 30
 339 s. Interestingly, for identical CNC-Br_{90%} concentrations range, the average emulsion drop
 340 diameter was higher for these simple inverse emulsions than for the present double emulsion
 341 system (Fig. S2, SI), whereas the opposite was expected since the rotor-stator homogenization
 342 is more powerful than the vibrating mixer process. The ability of the CNC to adsorb at the
 343 interface is therefore influenced by the presence of the direct inner emulsion and is not only
 344 governed by the amount of particles and the power of homogenization. Indeed, in a previous
 345 contribution, it has been demonstrated that 41 layers of CNC-Br_{90%} were present on the inverse

346 emulsions surface (Dupont, Laurichesse, et al., 2021), and in the present case only half this
347 value are adsorbed for each double emulsion drop. This difference could also be influenced
348 by the change in the physical-chemical characteristics such as its viscosity of the dispersed
349 phase, for instance.



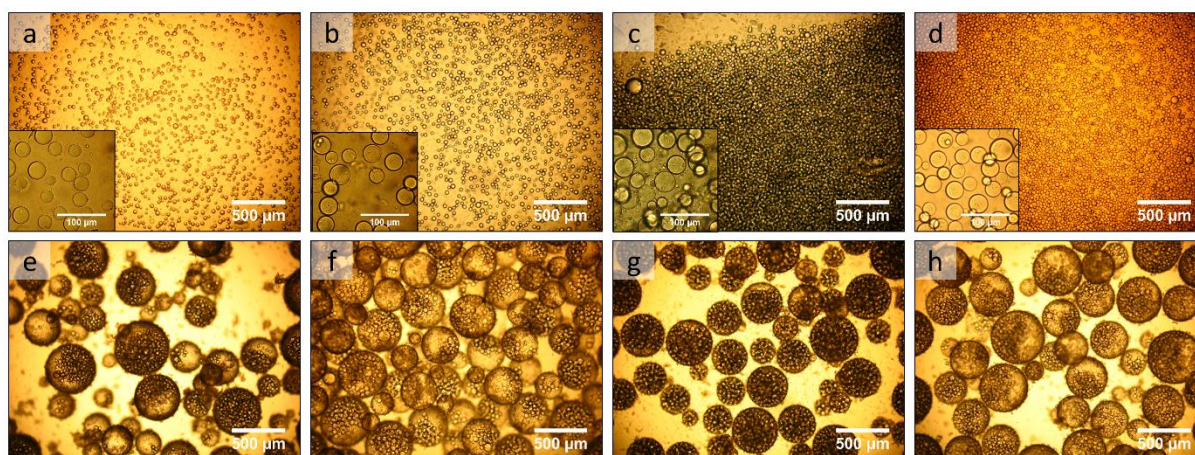
350

351 *Figure 6 : Left, Reverse drop diameter as a function of the amount of CNC-Br_{90%} in the organic*
352 *continuous phase. All the other parameters are kept constant: 25/75_{v/v} of direct emulsion/IPM, direct*
353 *emulsion IPM/aqueous phase ratio of 25/75_{v/v}, OEGMA 40 wt% no TEGDA. The linear variation*
354 *highlights the limited coalescence phenomenon occurring in this concentration range. The error bars*
355 *reflect the drops size distribution width (standard deviation). Right, optical microscopy shots of the*
356 *double emulsions with a) 5 g/L, b) 10 g/L, c) 15 g/L of CNC-Br_{90%}.*

357 Similarly to simple emulsions, a covering ratio could be extracted here from the slope of the
358 linear relationship between the inverse of the drop diameter and the concentration of particles
359 (Figure 6), acknowledging an average of 21 layers of CNC-Br_{90%} at the drops surface. These
360 multilayers are visible by optical microscopy, but more accurately by SEM (Figure 6, Figure 8),
361 showing a rough solid interface and the presence of CNC aggregates. Regarding the
362 morphology of the double emulsions, optical microscope observation showed that the inner
363 droplets tend to stack at the outer droplet interface (Figure 7B f). This phenomenon can be
364 explained by the van der Waals attractive interactions between the inner droplets and the wall
365 formed by the outer drop surface (Sengupta & Papadopoulos, 1992; Wen et al., 2004). This
366 observation is less visible when increasing the inner droplet volume fraction from 25 vol% to
367 50 vol%. Indeed, as the concentration of inner droplets increases, more volume of the drop is
368 occupied and the segregation becomes less noticeable (Figure 7B g).

369 The aqueous intermediate phase composition could be varied, without disturbing the simple
 370 and double emulsion stability (Figure 7A). Stable double emulsions were obtained with
 371 different OEGMA concentration of 10 wt% or 40 wt% (Figure 7B a, e and b, f). The addition of
 372 TEGDA as a cross-linker to the aqueous solution of OEGMA (concentration of 5 wt% and 35
 373 wt% respectively) did not impact neither the direct nor the double emulsion size (Figure 7B d,
 374 h, Figure 7A).

	Inner emulsion O/W volume fraction (v/v)	OEGMA (wt%)	TEGDA (wt%)	Inner emulsion diameter (μm)	Double emulsion diameter (μm)
a,e	25/75	10	0	33 ± 8	350 ± 89
b,f	25/75	40	0	35 ± 8	377 ± 107
c,g	50/50	40	0	38 ± 9	332 ± 94
d,h	25/75	35	5	34 ± 9	377 ± 88

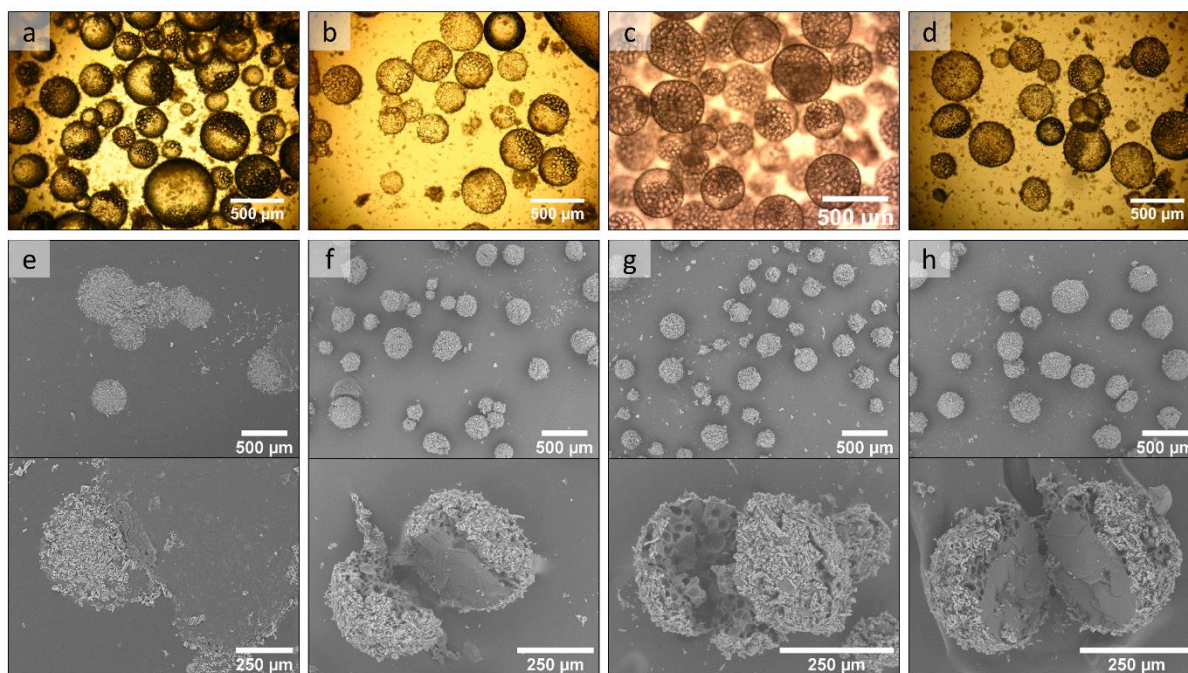


375
 376 *Figure 7: A) Formulation details of the emulsions presented below. B) Observation by optical microscopy*
 377 *of direct simple emulsion, 16 g/L CNC-Br_{20%}, at low oil volume fraction 25/75_{v/v} with varying OEGMA*
 378 *concentration a) 10 wt%, b) 40 wt%, c) with high oil volume fraction of 50/50_{v/v}, and d) in presence of a*
 379 *cross-linker (OEGMA/TEGDA 35/5 wt%). e-h) Respective double emulsions formulated with 20 g/L of*
 380 *CNC-Br_{90%}.*

381 382 3.3 Emulsion polymerization

383 Double emulsions were formulated with varying concentrations of OEGMA and TEGDA in the
 384 aqueous phase (10 wt%, 35 wt%-5wt%, 40wt%) and with two different loading fractions of
 385 inner droplets (25 vol% $n_{\text{inner}} \sim 250$, 50 vol% $n_{\text{inner}} \sim 500$). They were further polymerized by
 386 immersion in an oil bath at 75°C for 24 h. After polymerization, the emulsions were still
 387 dispersible in the supernatant IPM, contrary to observation of OEGMA/TEGDA polymerized
 388 emulsions initially stabilized by surfactants, which could only be redispersed in an aqueous
 389 medium (Stasse et al., 2020). Optical microscope observation showed a good stability of the

390 double emulsions upon heating and polymerization as the spherical morphology (Figure 8) and
391 the mean diameters of both inner droplets and outer drops were preserved (Figure 5). Both
392 internal droplets and external drops kept their average size distribution meaning that no
393 coalescence nor destabilization events occurred during the polymerization process. For low
394 loading fraction of inner droplets, the sticking phenomenon observed on non-polymerized
395 double emulsions is even more visible after polymerization, with a clear segregation of the
396 inner droplets on one side of the double emulsion, resulting in “Janus-like” polymer beads
397 (Figure 8 a, b, d). The phenomenon induced by the van der Waals attractive interactions was
398 most certainly enhanced by the creaming of the oil droplets within the drops during the 24h of
399 polymerization, which were performed without mixing. Morphologies were further
400 characterized by SEM, to assess the behavior of the capsules under a dry state and under
401 vacuum (Figure 8 e-h). As it was previously observed for polymerized inverse emulsions
402 (Dupont, Laurichesse, et al., 2021), the polymerized double emulsions presented on their
403 surface a dense cover of CNCs, which might participate in the good redispersibility of the
404 emulsions in IPM after polymerization. Almost all capsules could withstand the vacuum of the
405 SEM chamber (10^{-5} Pa) without collapsing, except for the lowest OEGMA concentration (10
406 wt%), most certainly because of the low filling in polymer inside the aqueous core (Figure 8 e).
407 For higher concentration in macromonomer, the objects kept their spherical shape with no
408 deformation induced by the vacuum. The capsules were hand-cut to inspect their inner core.
409 As expected, matrix morphology was observed, with visible cavities assessing for the presence
410 of the oil inner droplets (Figure 8 f, g, h). For low loading fractions of inner droplets about 25
411 vol% (Figure 8 f, g), the repartition of the cavities is clearly segmented with one part of the
412 capsule composed of full polymer and the other side concentrating the cavities made from the
413 presence of inner oil droplets. The increase in the inner droplet loading fraction from 25 vol%
414 to 50 vol% (Figure 8 g) is visible with an increase in the average number of cavities per capsule,
415 but also from the more even repartition of the cavities within the capsule, less subjected to the
416 microscopic segregation due to the van der Waals interactions.



417

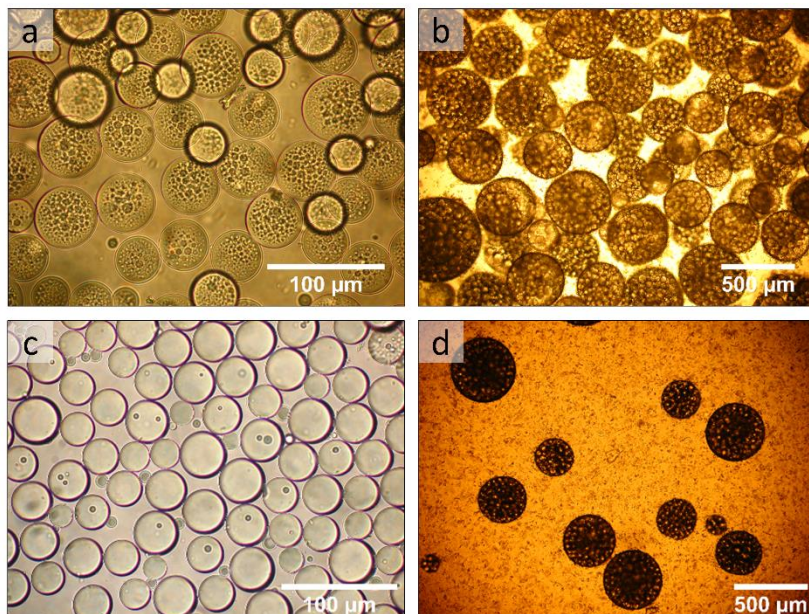
418 *Figure 8: Optical microscopy images of polymerized emulsions with 25 %v inner oil and a) 10 wt%*
 419 *OEGMA, b) 40 wt% OEGMA, d) 35 wt% OEGMA and 5 wt% TEGDA, and c) with 50 %v inner oil and*
 420 *40 wt% OEGMA. e-h) SEM pictures of the respective polymerized double emulsions, from a low and*
 421 *high magnification.*

422

423 3.4 Encapsulation efficiency

424 Double emulsions of OEGMA and TEGDA were efficiently stabilized by CNCs and further
 425 polymerized to obtain well-defined solid capsules. To increase the impact of these objects,
 426 their encapsulation ability was assessed as a proof of concept. The choice of encapsulated
 427 species was orientated towards fluorescent dyes (as models) which can be easily followed
 428 visually by confocal microscopy and quantified by UV-Vis spectrophotometry. The hydrophobic
 429 dye FY131SC, which is composed of "Solvent Red 175" dye, was chosen because of its very
 430 low solubility in water, with a maximum of absorption at 530 nm (full absorbance spectrum Fig.
 431 S3, SI). Its addition to IPM did not impact the emulsion formulation (Figure 9 a, b), since both
 432 droplets and drops average diameter were equal to $47 \pm 8 \mu\text{m}$ and $367 \pm 103 \mu\text{m}$ respectively
 433 without dye and to $38 \pm 9 \mu\text{m}$, $332 \pm 94 \mu\text{m}$ respectively in presence of FY131SC. The choice
 434 of the hydrophilic dye was subjected to optimization as it should have a different range of
 435 maximum of absorption and emission than the hydrophobic one, but also should not present
 436 interfacial properties in order not to interfere with the emulsion formulation. Therefore, toluidine

437 blue was preferred since it did not induce any change in the double emulsion formulation
438 (Figure 9 c, d), contrary to other dyes like methylene blue which contributed in increasing the
439 direct emulsion droplet diameter (Fig. S4, SI).

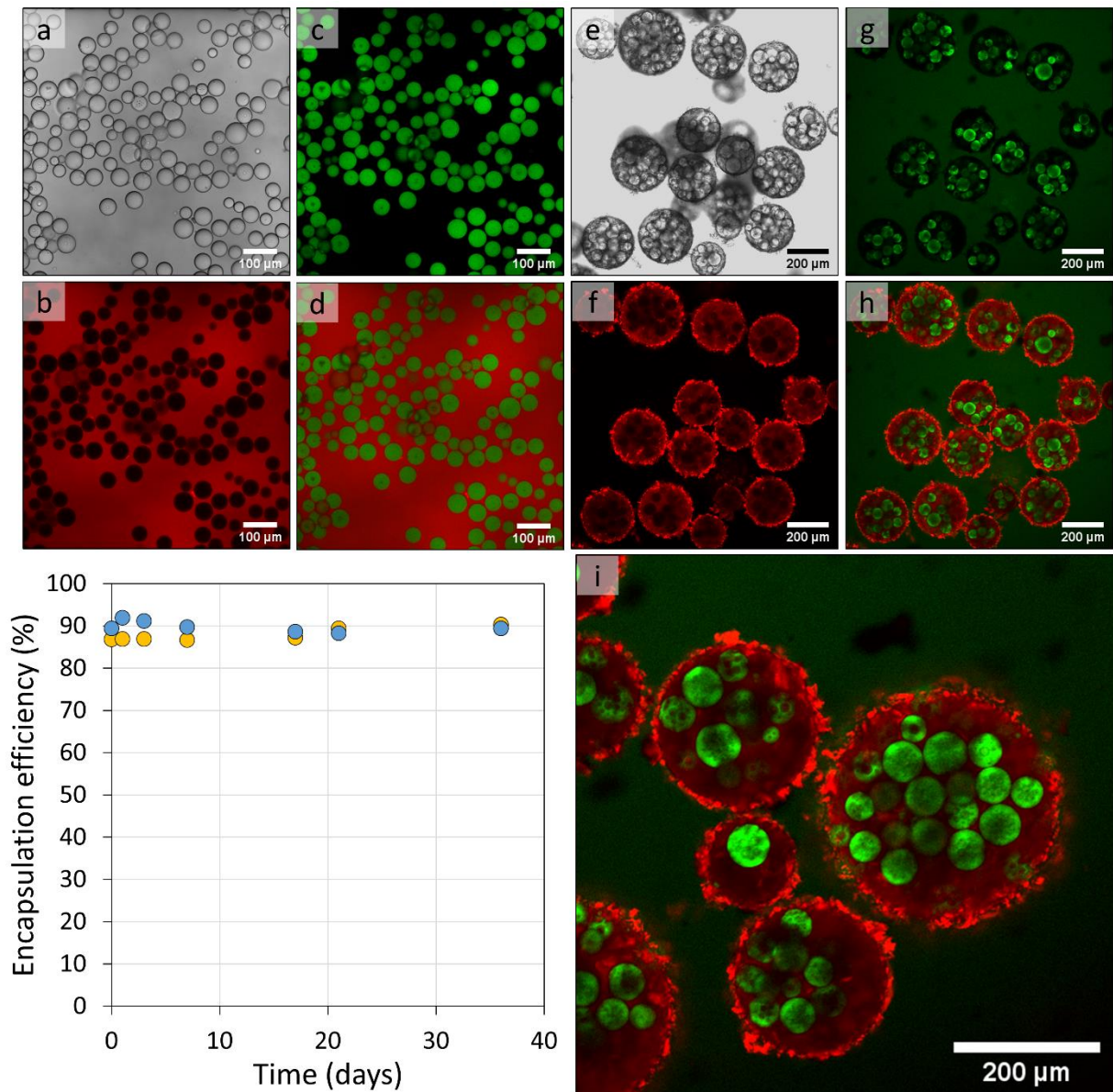


440

441 *Figure 9: Optical microscopy picture of direct (a,c) and corresponding double emulsion (b,d) in presence*
442 *of a, b) FY131SC and c, d) both FY131SC and toluidine blue.*

443 Confocal microscopy observation was performed on the stabilized double emulsion to verify
444 the effectiveness of the encapsulation and the special repartition of both dyes. Emulsions were
445 imaged by transmitted light and by fluorescence on a medium plane to enable the visualization
446 of the inner droplets. Each dye was imaged on a separate channel (hydrophobic FY131SC
447 appears in green and hydrophilic toluidine blue appears in red) and both signals were merged
448 by computation. The experiment shows that both toluidine blue and FY131SC are present in
449 the aqueous and oil phase of the direct emulsion respectively (Figure 10 i). For the double
450 emulsion, the inner droplets can be easily distinguished from the intermediate polymerized
451 phase as they are selectively labelled by the hydrophobic dye (Figure 10 g). The polymer
452 phase, which appears red is also selectively stained by the hydrophilic dye (Figure 10 f).
453 Another feature which might be of interest to notice is the light green staining in the background
454 assessing for the presence of the hydrophobic dye in the continuous phase, and indicating the
455 occurrence of leakage following the second emulsification. However, as the fluorescence
456 intensity in the background is low compared to the inner droplets, the concentration of dye in

457 the continuous phase can be considered as low and therefore that the leakage is not too
 458 pronounced.



459

460 *Figure 10: Pictures – Confocal microscopy image of a direct emulsion with toluidine blue and FY131SC,*
 461 *a) in bright field, b) red channel, c) green channel and d) superimposition of the red and green channels.*
 462 *Toluidine blue and FY131SC are revealed by the red and green channels respectively. e-h) Resulting*
 463 *double emulsion with toluidine blue and FY131SC, and i) close-up at higher magnification. Images were*
 464 *taken at a given z. Graph – Encapsulation efficiency of double emulsions of OEGMA and TEGDA, with*
 465 *(blue) and without (yellow) polymerization. The point at $t = 0$ corresponds to the sample right after*
 466 *formulation, and $t = 1$ day corresponds to the sample after 24h of polymerization for the blue curve.*

467 In order to corroborate this hypothesis, and quantify the amount of dye that could effectively
 468 be encapsulated within the double emulsion-templated capsules, indirect encapsulation
 469 efficiency measurement was performed. Double emulsions with FY131SC in the inner oil
 470 droplets were formulated with 35 wt% OEGMA and 5 wt% TEGDA in the intermediate phase.

471 One double emulsion was kept at ambient temperature as a control experiment, while the other
472 was polymerized at 75°C for 24h. The presence of dye in the IPM continuous phase was
473 measured over time by UV-Visible spectrophotometry. Thanks to Eq. 4, the encapsulation
474 efficiency was calculated for both non-polymerized and polymerized double emulsions. Both
475 double emulsions showed good encapsulation efficiency of about 90% directly after
476 formulation (Figure 10). After polymerization, almost no dye could be detected into the
477 continuous phase, giving an estimated encapsulation efficiency of about 90% (Figure 10, blue).
478 A control experiment has been additionally performed, and has shown that the hydrophobic
479 dye does not degrade when submitted to 75°C during 24h (Figure S5, SI). Hence, the absence
480 of dye detection into the continuous phase can be accurately linked to the good encapsulation
481 efficiency and not to a dye leakage followed by degradation. This encapsulation efficiency
482 value remained constant over a month, for both the non-polymerized and the polymerized
483 double emulsions. Hence, the polymerization process of the double emulsion, even in harsh
484 conditions of temperature, did not affect neither the stability of the system nor the
485 encapsulation efficiency of the hydrophobic dye, which is promising regarding active-delivery
486 applications.

487

488 **4. Conclusion**

489 We have shown that O/W/O double emulsions could be stabilized using solely brominated
490 cellulose nanocrystals. Their modification rate was directly linked to the reaction time, and
491 monitors the ability of the particles to stabilize either direct or inverse emulsion. Double
492 emulsion could be formulated using two batches of CNCs, one with a low modification rate
493 about 20% and the other with a high modification rate of 90%. Isopropyl myristate, a polar
494 biocompatible oil was used as inner oil phase and as continuous medium. The aqueous
495 intermediate phase was composed of oligoethylene glycol derivatives, namely hydroxyl
496 oligoethylene glycol methacrylate and tetraethylene glycol diacrylate. For the first time, a
497 double emulsion stabilized solely by CNCs was polymerized. The aqueous intermediate phase
498 was polymerized by free radical polymerization, and led to solid matrix capsules, which

499 conserved the initial emulsion characteristics, with tunable inner droplets content, and varying
500 monomer(s) fraction. Finally, their use as double encapsulation vessels was investigated. Both
501 hydrophobic and hydrophilic dyes could be encapsulated within the inner droplets and the
502 intermediate phase respectively. The encapsulation efficiency of the hydrophilic dye was equal
503 to 100% given the insolubility of the dye in the other phases. For the hydrophobic dye, it was
504 measured approximately equal to 90% indicating promising results to further extend their
505 application to controlled delivery.

506

507 **Acknowledgements**

508 The authors would like to thank Emmanuel Ibarboure for his help with fluorescence microscopy
509 imaging of the stained emulsions.

510 This work was supported by the French “Fondation Bordeaux Université” and the “Fonds
511 Ernest Solvay” supported by “Fondation Roi Baudouin”.

512 **References**

- 513 Arditty, S, Whitby, C. P., Binks, B. P., Schmitt, V., & Leal-Calderon, F. (2003). Some general
514 features of limited coalescence in solid-stabilized emulsions. *Eur. Phys. J. E*, *11*, 273–
515 281. <https://doi.org/10.1140/epje/i2003-10018-6>
- 516 Arditty, Stéphane, Schmitt, V., Giermanska-Kahn, J., & Leal-Calderon, F. (2004). Materials
517 based on solid-stabilized emulsions. *Journal of Colloid and Interface Science*, *275*, 659–
518 664. <https://doi.org/10.1016/j.jcis.2004.03.001>
- 519 Brand, J., Pecastaings, G., & Sèbe, G. (2017). A versatile method for the surface tailoring of
520 cellulose nanocrystal building blocks by acylation with functional vinyl esters.
521 *Carbohydrate Polymers*, *169*, 189–197. <https://doi.org/10.1016/j.carbpol.2017.03.077>
- 522 Cunha, A. G., Mougel, J.-B., Cathala, B., Berglund, L. A., & Capron, I. (2014). Preparation of
523 double Pickering emulsions stabilized by chemically tailored nanocelluloses. In
524 *Langmuir* (Vol. 30). <https://doi.org/10.1021/la5017577>
- 525 Deng, Z., Jung, J., Simonsen, J., & Zhao, Y. (2018). Cellulose nanocrystals Pickering
526 emulsion incorporated chitosan coatings for improving storability of postharvest Bartlett
527 pears (*Pyrus communis*) during long-term cold storage. *Food Hydrocolloids*, *84*, 229–
528 237. <https://doi.org/10.1016/J.FOODHYD.2018.06.012>
- 529 Destribats, M., Gineste, S., Laurichesse, E., Tanner, H., Leal-Calderon, F., Héroguez, V., &
530 Schmitt, V. (2014). Pickering Emulsions: What Are the Main Parameters Determining
531 the Emulsion Type and Interfacial Properties? *Langmuir*, *30*, 9313–9326.
532 <https://doi.org/10.1021/la501299u>
- 533 Ding, S., Serra, C. A., Vandamme, T. F., Yu, W., & Anton, N. (2019). Double emulsions
534 prepared by two-step emulsification: History, state-of-the-art and perspective. In *Journal*
535 *of Controlled Release* (Vol. 295, pp. 31–49). Elsevier B.V.
536 <https://doi.org/10.1016/j.jconrel.2018.12.037>
- 537 Dupont, H., Fouché, C., Dourges, M.-A., Schmitt, V., & Héroguez, V. (2020). Polymerization
538 of cellulose nanocrystals-based Pickering HIPE towards green porous materials.
539 *Carbohydrate Polymers*, *243*, 116411. <https://doi.org/10.1016/j.carbpol.2020.116411>

540 Dupont, H., Laurichesse, E., Héroguez, V., & Schmitt, V. (2021). Green Hydrophilic Capsules
541 from Cellulose Nanocrystal-Stabilized Pickering Emulsion Polymerization: Morphology
542 Control and Spongelike Behavior. *Biomacromolecules*, 22(8), 3497–3509.
543 <https://doi.org/10.1021/acs.biomac.1c00581>

544 Dupont, H., Maingret, V., Schmitt, V., & Héroguez, V. (2021). New Insights into the
545 Formulation and Polymerization of Pickering Emulsions Stabilized by Natural Organic
546 Particles. *Macromolecules*, 54(11), 4945–4970.
547 <https://doi.org/10.1021/acs.macromol.1c00225>

548 Finkle, P., Draper, H. D., & Hildebrand, J. H. (1923). The Theory of Emulsification. *Journal of*
549 *American Chemical Society*, 45(12), 2780–2788. <https://pubs.acs.org/sharingguidelines>

550 Gestranus, M., Stenius, P., Kontturi, E., Sjöblom, J., & Tammelin, T. (2017). Phase
551 behaviour and droplet size of oil-in-water Pickering emulsions stabilised with plant-
552 derived nanocellulosic materials. *Colloids and Surfaces A: Physicochemical and*
553 *Engineering Aspects*, 519, 60–70. <https://doi.org/10.1016/j.colsurfa.2016.04.025>

554 Gonzalez Ortiz, D., Pochat-Bohatier, C., Cambedouzou, J., Bechelany, M., & Miele, P.
555 (2020). Current Trends in Pickering Emulsions: Particle Morphology and Applications.
556 *Engineering*. <https://doi.org/10.1016/j.eng.2019.08.017>

557 Guo, J., Du, W., Gao, Y., Cao, Y., & Yin, Y. (2017). Cellulose nanocrystals as water-in-oil
558 Pickering emulsifiers via intercalative modification. *Colloids and Surfaces A:*
559 *Physicochemical and Engineering Aspects*, 529, 634–642.
560 <https://doi.org/10.1016/j.colsurfa.2017.06.056>

561 Hedjazi, S., & Razavi, S. H. (2018). A comparison of Canthaxanthine Pickering emulsions,
562 stabilized with cellulose nanocrystals of different origins. *International Journal of*
563 *Biological Macromolecules*, 106, 489–497.
564 <https://doi.org/10.1016/j.ijbiomac.2017.08.030>

565 Kalashnikova, I., Bizot, H., Cathala, B., & Capron, I. (2011). New Pickering Emulsions
566 Stabilized by Bacterial Cellulose Nanocrystals. *Langmuir*, 27(12), 7471–7479.
567 <https://doi.org/10.1021/la200971f>

568 Lee, K.-Y., Blaker, J. J., Murakami, R., Heng, J. Y. Y., & Bismarck, A. (2013). *Phase*
569 *Behavior of Medium and High Internal Phase Water-in-Oil Emulsions Stabilized Solely*
570 *by Hydrophobized Bacterial Cellulose Nanofibrils*. <https://doi.org/10.1021/la4032514>

571 Mackie, A., Gourcy, S., Rigby, N., Moffat, J., Capron, I., & Bajka, B. (2019). The fate of
572 cellulose nanocrystal stabilised emulsions after simulated gastrointestinal digestion and
573 exposure to intestinal mucosa †. *Nanoscale*, *11*. <https://doi.org/10.1039/c8nr05860a>

574 Matos, M., Timgren, A., Sjöö, M., Dejmek, P., & Rayner, M. (2013). Preparation and
575 encapsulation properties of double Pickering emulsions stabilized by quinoa starch
576 granules. *Colloids and Surfaces A: Physicochemical and Engineering Aspects*, *423*,
577 147–153. <https://doi.org/10.1016/j.colsurfa.2013.01.060>

578 Meng, T., Gao, X., Zhang, J., Yuan, J., Zhang, Y., & He, J. (2008). Graft copolymers
579 prepared by atom transfer radical polymerization (ATRP) from cellulose. *Polymer*, *50*,
580 447–454. <https://doi.org/10.1016/j.polymer.2008.11.011>

581 Morandi, G., Heath, L., & Thielemans, W. (2009). Cellulose Nanocrystals Grafted with
582 Polystyrene Chains through Surface Initiated Atom Transfer Radical Polymerization (SI-
583 ATRP). *Langmuir*, *25*(14), 5. <https://doi.org/10.1021/la900452a>

584 Pan, J., Yin, Y., Gan, M., Meng, M., Dai, X., Wu, R., Shi, W., & Yan, Y. (2015). Fabrication
585 and evaluation of molecularly imprinted multi-hollow microspheres adsorbents with
586 tunable inner pore structures derived from templating Pickering double emulsions.
587 *Chemical Engineering Journal*, *266*, 299–308.
588 <https://doi.org/10.1016/J.CEJ.2014.11.126>

589 Pickering, S. U. (1907). CXCVI.—Emulsions. *Journal of the Chemical Society, Transactions*,
590 *91*, 2001–2021.

591 Ramsden, W. (1904). Separation of solids in the surface-layers of solutions and
592 'suspensions' (observations on surface-membranes, bubbles, emulsions, and
593 mechanical coagulation).—Preliminary account. *Proceedings of the Royal Society of*
594 *London*, *72* (477-48), 156–164.

595 Sarkar, A., & Dickinson, E. (2020). Sustainable food-grade Pickering emulsions stabilized by

596 plant-based particles. *Current Opinion in Colloid & Interface Science*, 49, 69–81.
597 <https://doi.org/10.1016/j.cocis.2020.04.004>

598 Schmitt, V., Destribats, M., & Backov, R. (2014). Colloidal particles as liquid dispersion
599 stabilizer: Pickering emulsions and materials thereof. *Comptes Rendus Physique*, 15(8–
600 9), 761–774. <https://doi.org/10.1016/j.crhy.2014.09.010>

601 Sengupta, A. K., & Papadopoulos, K. D. (1992). van der Waals Interaction between a Colloid
602 and the Wall of Its Host Spherical Cavity. *Journal of Colloid and Interface Science*,
603 152(2), 534–542.

604 Spyropoulos, F., Duffus, L. J., Smith, P., & Norton, I. T. (2019). Impact of Pickering
605 Intervention on the Stability of W1/O/W2 Double Emulsions of Relevance to Foods.
606 *Langmuir*, 35, 15137–15150. <https://doi.org/10.1021/acs.langmuir.9b01995>

607 Stasse, M., Laurichesse, E., Vandroux, M., Ribaut, T., Héroguez, V., & Schmitt, V. (2020).
608 Cross-linking of double oil-in-water-in-oil emulsions: A new way for fragrance
609 encapsulation with tunable sustained release. *Colloids and Surfaces A:
610 Physicochemical and Engineering Aspects*, 607, 125448.
611 <https://doi.org/10.1016/j.colsurfa.2020.125448>

612 Wen, L., Cheng, J., Zou, H., Zhang, L., Chen, J., & Papadopoulos, K. D. (2004). van der
613 Waals Interaction between Internal Aqueous Droplets and the External Aqueous Phase
614 in Double Emulsions. *Langmuir*, 20, 8391–8397. <https://doi.org/10.1021/la049353s>

615 Werner, A., Schmitt, V., Sèbe, G., & Héroguez, V. (2019). Convenient Synthesis of Hybrid
616 Polymer Materials by AGET-ATRP Polymerization of Pickering Emulsions Stabilized by
617 Cellulose Nanocrystals Grafted with Reactive Moieties. *Biomacromolecules*, 20(1), 490.
618 <https://doi.org/10.1021/acs.biomac.8b01482>

619 Wiley, R. M. (1954). Limited coalescence of oil droplets in coarse oil-in-water emulsions.
620 *Journal of Colloid Science*, 9(5), 427–437. [https://doi.org/10.1016/0095-8522\(54\)90030-
621 6](https://doi.org/10.1016/0095-8522(54)90030-6)

622 Zhang, Z., Tam, K. C., Wang, X., & Sèbe, G. (2018). Inverse Pickering Emulsions Stabilized
623 by Cinnamate Modified Cellulose Nanocrystals as Templates to Prepare Silica

624 Colloidosomes. *ACS Sustainable Chemistry and Engineering*, 6(2), 2583–2590.

625 <https://doi.org/10.1021/acssuschemeng.7b04061>

626